JOURNAL OF GUIDANCE, CONTROL, AND DYNAMICS
Vol. 18, No. 6, November–December 1995

Modeling of Translational Motion Between Two Flexible Bodies Connected via Three Points

Sivakumar S. K. Tadikonda*
Grumman Corporation, Reston, Virginia 22091

A dynamic model is presented in this paper for modeling the translation of a flexible body over another flexible body with three load transmission points between them. The three contact points on one of the bodies continuously change as one body translates with respect to the other. No software tools currently exist for simulating the dynamic response of this two-body system. In the present model, six degrees of freedom are allowed between the two bodies and then contacts are modeled using constraints that account for the relative motion. The small, elastic deformation of each body is modeled using the method of assumed modes. Numerical results presented demonstrate the dynamic interactions. The steps needed for implementation in multibody dynamics codes are outlined. The Mobile Transporter-Space Station system is a direct application for the present model.

I. Introduction

DYNAMICS formulations[1–3] and software analysis tools such as TREETOPS[4] and DISCOS[5] model the relative motion between two bodies in an articulated, flexible multibody system through a hinge that can permit up to six degrees of freedom (DOFs). In such models, the relative translational motion is defined as that occurring between two points, one each fixed in each of the bodies, and the relative rotational motion as that between two reference frames, one each attached at the same two points in the respective bodies. A typical hinge definition is shown in Fig. 1. This definition facilitates the modeling of open-loop, articulated flexible multibody systems such as the Shuttle Remote Manipulator System (SRMS) and typical spacecraft with articulating flexible solar arrays. In the case of closed-loop systems, a cut joint is introduced to render the system open loop, with the joint definition the same as above, and then loop closure constraints are imposed.

A consequence of the above definition for a joint connecting two bodies is that the dynamics of a flexible beam translating over two rigid supports, studied by Buffinton and Kane,[6] cannot be modeled using the above formulations or software. This is because the points on the flexible beam that are in contact with the two rigid supports continuously change as the beam translates. The translation joint modeling in Refs. 1–5 assumes that the translation occurs along a rigid appendage, although the bodies themselves may be flexible. Although not incorporated into TREETOPS,[4] Li and Likins[7] extended the approach of Singh et al.[4] to include travel along a curved flexible path, with a single point contact between the flexible guide and the body traveling on it. Hwang and Haug[8] modeled one- and two-point contacts between two flexible bodies but presented numerical results only for the single-point contact case.

Another system that cannot be modeled using the above joint definition alone is shown in Fig. 2. Body j and body $L(j)$ in this figure are in contact at three locations and body j travels over a pair of parallel tracks that are fixed to body $L(j)$. Two of the three contacts between the bodies occur over one rail whereas the third contact occurs over the other rail. Both the bodies are flexible. The interaction dynamics with multipoint contact between flexible bodies and with a relative DOF has not been modeled in the literature and cannot be simulated using the available multibody dynamics software.

Single- and multipoint contact studies in the literature[9–12] investigate how a flexible body will react to a given set of moving point loads. However, when the force exerted on the flexible body is due to the motion of a connected body, the motion of the flexible body will have an effect on the connected body according to Newton's third law, and such an interaction dynamics is not modeled in Refs. 9–12. References 6 and 10 considered continuum representations for component body modal models whereas Refs. 8, 9, 11, and 12 consider finite element representations.

A formulation is presented here for modeling the dynamics of the system shown in Fig. 2 in a multibody form, so that it can be implemented in existing dynamics software. The three-point contact is modeled through the imposition of a set of constraints. The body elasticity is modeled using the method of assumed modes, and the method is applicable regardless of whether the component mode set is obtained from a continuum or a finite element representation of the component body flexibility.

The following nomenclature is used in this paper. Boldface italic characters represent vectors; subscripts f, p, q, A_1, A_2, B_1, B_2, C_1, and C_2 on these vectors refer to nodal association. Superscripts j and $L(j)$ refer to body identities, with body $L(j)$ being the body that is directly inboard of body j, and superscript T denotes the transpose. The vector $\boldsymbol{R}^j$ denotes the position with respect to an inertial frame and $\boldsymbol{r}^j$ denotes the position with respect to the body frame. Body reference frames are identified by $\mathbf{b}$ and a subscript on this boldfaced character refers to a body with that index. Using this nomenclature, for example, $\boldsymbol{r}_p^{L(j)}$ denotes the vector defining the undeformed location of the p node on body $L(j)$ with respect to the origin of $\mathbf{b}_{L(j)}$.

II. Recursive Kinematics and Unconstrained Dynamics

The description of a generic hinge connecting two bodies shown in Fig. 1 forms the basis for the system kinematics and dynamics formulation and the associated constraints. In Fig. 1, body j and body $L(j)$ are connected by hinge j. This generic hinge can permit up to six rigid-body DOFs.

Let the undeformed configuration of any point on body j be defined by a vector $\boldsymbol{r}^j$ with respect to the body frame $\mathbf{b}_j$. The time-varying elastic deformation at this location is represented by $\boldsymbol{u}^j(\boldsymbol{r}^j, t)$, measured with respect to $\mathbf{b}_j$ and is assumed to be small, and t denotes time. The origins of the reference frames $\mathbf{b}_j$ and $\mathbf{b}_{L(j)}$ are located by the vectors $\boldsymbol{R}_f^j$ and $\boldsymbol{R}_f^{L(j)}$, respectively, with respect to an inertial frame. The translational displacement of node q on body j with respect to node p on body $L(j)$ is indicated by the vector ${}^{L(j)}\mathbf{y}^j$. This translation is defined in the frame located at node p on body $L(j)$.

The vector locating an arbitrary elemental mass dm on body j with respect to an inertial frame is given by

$$\boldsymbol{R}^j = \boldsymbol{R}_f^j + \boldsymbol{r}^j + \boldsymbol{u}^j(\boldsymbol{r}^j, t) \tag{1}$$

Received June 15, 1993; revision received Feb. 17, 1995; accepted for publication March 21, 1995.

*Senior Flight Systems Engineer, Space Station Integration Division; currently Senior Principal Engineer, McDonnell Douglas Aerospace, 7404 Executive Place, Seabrook, MD 20706. Member AIAA.

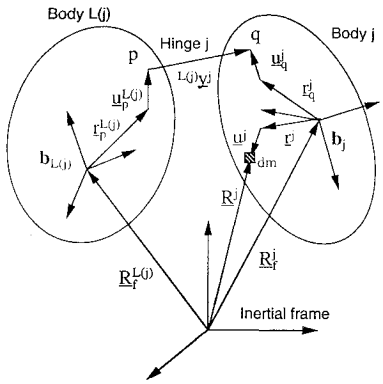

Fig. 1 Recursive kinematic description of generic hinge.

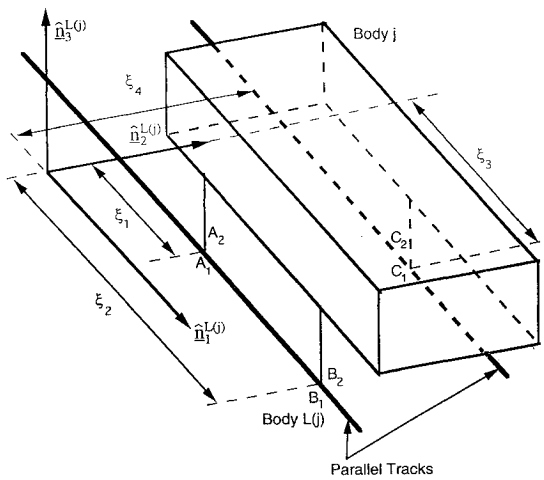

Fig. 2 Three-point contact model.

A shorthand notation $\boldsymbol{u}_q^j = \boldsymbol{u}^j(\boldsymbol{r}_q^j, t)$, etc., will be employed in the rest of the paper, consistent with the nomenclature, for brevity. A recursive kinematic expression can be written, from Fig. 1, as

$$\boldsymbol{R}_f^j = \boldsymbol{R}_p^{L(j)} + {}^{L(j)}\boldsymbol{y}^j - \left(\boldsymbol{r}_q^j + \boldsymbol{u}_q^j\right) \tag{2}$$

where

$$\boldsymbol{R}_p^{L(j)} = \boldsymbol{R}_f^{L(j)} + \boldsymbol{r}_p^{L(j)} + \boldsymbol{u}_p^{L(j)} \tag{3}$$

Differentiation of Eq. (1) with respect to time yields the expression for the velocity of dm:

$$\dot{\boldsymbol{R}}^j = \dot{\boldsymbol{R}}_f^j + \boldsymbol{\omega}^j \times (\boldsymbol{r}^j + \boldsymbol{u}^j) + \frac{\partial}{\partial t}(\boldsymbol{u}^j) \tag{4}$$

in which $\boldsymbol{\omega}^j$ represents the angular velocity of the body reference frame $\mathbf{b}_j$ and is defined recursively as

$$\boldsymbol{\omega}^j = \boldsymbol{\omega}^{L(j)} + \frac{\partial}{\partial t}\left(\boldsymbol{u}_p'^{L(j)}\right) + {}^{L(j)}\boldsymbol{\omega}^j - \frac{\partial}{\partial t}\left(\boldsymbol{u}_q'^j\right) \tag{5}$$

In Eq. (4), the overdot and $\partial/\partial t$ correspond to differentiation with respect to time in the inertial and local frames, respectively. In Eq. (5), primes denote small rotations due to elastic motions. The relative rigid-body angular velocity across hinge j is indicated by ${}^{L(j)}\boldsymbol{\omega}^j$ in Eq. (5) and can be expressed in terms of a selected Euler sequence as

$${}^{L(j)}\boldsymbol{\omega}^j = \sum_{i=1}^{\mathrm{NR}_j} \boldsymbol{l}_i^j(\{\theta^j\})\dot{\theta}_i^j \tag{6}$$

where $\{\theta^j\} = [\theta_1^j \cdots \theta_{\mathrm{NR}_j}^j]^T$ is a column matrix containing the Euler angles, $\dot{\theta}_i^j (i = 1, \ldots, \mathrm{NR}_j)$ are the corresponding angular rates, $\boldsymbol{l}_i^j (i = 1, \ldots, \mathrm{NR}_j)$ represent the unit vectors along the Euler axes for the selected sequence, and NR_j represents the number of rotational DOFs at hinge j. Let

$$\boldsymbol{\Gamma}^j = \boldsymbol{r}^j + \boldsymbol{u}^j - \boldsymbol{r}_q^j - \boldsymbol{u}_q^j \tag{7}$$

$$\boldsymbol{\omega}_p^{L(j)} = \boldsymbol{\omega}^{L(j)} + \frac{\partial}{\partial t}\left(\boldsymbol{u}_p'^{L(j)}\right) \tag{8}$$

Substitution of Eqs. (7) and (8) and a differentiated form of Eq. (2) into Eq. (4) yields

$$\dot{\boldsymbol{R}}^j = \dot{\boldsymbol{R}}_p^{L(j)} + \boldsymbol{\omega}_p^{L(j)} \times {}^{L(j)}\boldsymbol{y}^j + \frac{\partial}{\partial t}\left({}^{L(j)}\boldsymbol{y}^j\right) + \boldsymbol{\omega}^j \times \boldsymbol{\Gamma}^j + \frac{\partial}{\partial t}\left(\boldsymbol{u}^j - \boldsymbol{u}_q^j\right) \tag{9}$$

The rigid-body translational velocity $(\partial/\partial t)({}^{L(j)}\boldsymbol{y}^j)$ across hinge j can be expressed in terms of the translational DOFs across hinge j as

$$\frac{\partial}{\partial t}\left({}^{L(j)}\boldsymbol{y}^j\right) = \sum_{i=1}^{\mathrm{NT}_j} \boldsymbol{g}_i^{L(j)} \dot{y}_i^j \tag{10}$$

in which $\boldsymbol{g}_i^{L(j)} (i = 1, \ldots, \mathrm{NT}_j)$ are the unit vectors defined in the reference frame located at the p node on body $L(j)$, y_i^j are the time-dependent translational coordinates, $\dot{y}_i^j$ are the associated translational rates, and NT_j represents the number of translational DOFs across hinge j.

The elastic displacement $\boldsymbol{u}^j$ at any location $\boldsymbol{r}^j$ in $\mathbf{b}_j$ can be expressed using the assumed modes method[13] as

$$\boldsymbol{u}^j(\boldsymbol{r}^j, t) = \sum_{i=1}^{\mathrm{NM}_j} \boldsymbol{\phi}_i^j(\boldsymbol{r}^j)\eta_i^j(t) \tag{11}$$

where the $\boldsymbol{\phi}_i^j$ $(i = 1, \ldots, \mathrm{NM}_j)$ represent the assumed mode shape vectors, $\eta_i^j(t)$ are their time-dependent amplitudes, and NM_j is the number of retained modes for body j in the modal expansion. Differentiation of Eq. (11) with respect to time in body frame $\mathbf{b}_j$ yields

$$\frac{\partial}{\partial t}[\boldsymbol{u}^j(\boldsymbol{r}^j, t)] = \sum_{i=1}^{\mathrm{NM}_j} \boldsymbol{\phi}_i^j(r^j)\dot{\eta}_i^j \tag{12}$$

The number of DOFs of the unconstrained system then is

$$N = \sum_{j=1}^{\mathrm{NB}} (\mathrm{NT}_j + \mathrm{NR}_j + \mathrm{NM}_j) \tag{13}$$

where NB is the total number of bodies. The equations of motion for the unconstrained system can be obtained in the standard form

$$M(\nu)\ddot{\nu} + G(\nu, \dot{\nu}) = F \tag{14}$$

where ν is an $N \times 1$ column matrix of generalized coordinates, M is the $N \times N$ mass matrix, G is the $N \times 1$ column matrix containing linear and nonlinear terms in ν and $\dot{\nu}$, and F represents the $N \times 1$ column matrix of generalized forces.

In the context of the problem on hand, shown in Fig. 2, the kinematic expressions in Eqs. (9–12), and the definition of a generic hinge (Fig. 1), a question arises as to what a p node on body $L(j)$ is. This is because the hinge definition requires that both p and q nodes have no rigid-body translation with respect to the respective body frames. However, when body j in Fig. 2 translates over body $L(j)$, the contact points A_1, B_1, and C_1 on body $L(j)$ corresponding to (fixed) A_2, B_2, and C_2 on body j continuously change. That is, A_1, B_1, and C_1 represent the contact points on body $L(j)$ at any given instant and hence are not fixed with respect to the body frame $\mathbf{b}_{L(j)}$; thus, none of these nodes can be selected as the p node.

The method proposed here consists of the following steps: 1) retaining the hinge definition shown in Fig. 1 and the recursive kinematic equations presented above by defining the p and q nodes to be materially fixed points and then 2) imposing the constraints

for the three contacts between body j and $L(j)$ while properly accounting for the translation with respect to the body frame $\mathbf{b}_{L(j)}$. These p and q nodes do not coincide with any of the contact points. In fact, the p node must be selected as the reference point with respect to which body j motion must be controlled. All six DOFs will be permitted across hinge j, i.e., $\mathrm{NT}_j = \mathrm{NT}_j = 3$. Of these, five DOFs will be eliminated through the constraints formed for the three contacts so that only one DOF exists between the body pair j and $L(j)$. This is described in the next section.

III. Constraint Equations

Recall that six relative rigid-body DOFs have been allowed between the body pair j and $L(j)$ in Sec. II. Here, we introduce four additional configuration variables—ξ_1, ξ_2, ξ_3, and ξ_4, defined as shown in Fig. 2—for representing the contact. The position constraints for the contacts between these bodies imply nine scalar constraints. The new configuration variables introduced here can be eliminated using four of these constraint equations. The six DOFs between the body pair j and $L(j)$ subject to the remaining five constraints yield the desired one relative DOF. The constraints are formed as described below.

Consider the three-point contact shown in Fig. 2. The three nodes on body $L(j)$ that are in contact with body j are denoted by A_1, B_1, and C_1, and A_2, B_2, and C_2 denote their counterparts on body j. Using the kinematic description in Sec. II, the position constraints for the contact between body j and body $L(j)$ can be written as

$$\boldsymbol{R}_f^j + \boldsymbol{r}_{A_2}^j + \boldsymbol{u}_{A_2}^j - \boldsymbol{R}_f^{L(j)} - \boldsymbol{r}_{A_1}^{L(j)} - \boldsymbol{u}_{A_1}^{L(j)} = \mathbf{0} \tag{15}$$

$$\boldsymbol{R}_f^j + \boldsymbol{r}_{B_2}^j + \boldsymbol{u}_{B_2}^j - \boldsymbol{R}_f^{L(j)} - \boldsymbol{r}_{B_1}^{L(j)} - \boldsymbol{u}_{B_1}^{L(j)} = \mathbf{0} \tag{16}$$

$$\boldsymbol{R}_f^j + \boldsymbol{r}_{C_2}^j + \boldsymbol{u}_{C_2}^j - \boldsymbol{R}_f^{L(j)} - \boldsymbol{r}_{C_1}^{L(j)} - \boldsymbol{u}_{C_1}^{L(j)} = \mathbf{0} \tag{17}$$

It is assumed that contact across all the point pairs is maintained at all times. Equations (2) and (3) can be used to eliminate $\boldsymbol{R}_f^j - \boldsymbol{R}_f^{L(j)}$ from Eqs. (15–17). For the nonplanar motion of the body pair considered here, Eqs. (15–17) correspond to nine scalar constraints. Note that the three closed loops represented in Eqs. (15–17) are between the same two flexible bodies, and loop closures involve points that are moving with respect to $\mathbf{b}_{L(j)}$. Such a topology cannot be modeled using TREETOPS[4] or DISCOS.[5]

The velocity constraint corresponding to the contact across the nodes A_1 and A_2 can be obtained by differentiating Eq. (15) with respect to time in the inertial frame, as

$$\dot{\boldsymbol{R}}_f^{L(j)} + \boldsymbol{\omega}^{L(j)} \times \left(\boldsymbol{r}_{A_1}^{L(j)} + \boldsymbol{u}_{A_1}^{L(j)}\right) + \frac{\partial^{L(j)}}{\partial t}\left(\boldsymbol{r}_{A_1}^{L(j)} + \boldsymbol{u}_{A_1}^{L(j)}\right)$$

$$- \dot{\boldsymbol{R}}_f^j - \boldsymbol{\omega}^j \times \left(\boldsymbol{r}_{A_2}^j + \boldsymbol{u}_{A_2}^j\right) - \frac{\partial^j}{\partial t}\left(\boldsymbol{u}_{A_2}^j\right) = \mathbf{0} \tag{18}$$

The body frame dependency for the time derivative in the local frame is indicated by the superscript in $\partial^{L(j)}/\partial t$ and $\partial^j/\partial t$. Since the instantaneous contact point A_1 is translating with respect to $\mathbf{b}_{L(j)}$, the local time derivative of $\boldsymbol{r}_{A_1}^{L(j)}$ is not a null vector. Let $\hat{\boldsymbol{n}}_1^{L(j)}$ be the unit vector along the nominal translational direction in $\mathbf{b}_{L(j)}$. Then,

$$\frac{\partial^{L(j)}}{\partial t}\left(\boldsymbol{r}_{A_1}^{L(j)}\right) = \dot{\xi}_1 \hat{\boldsymbol{n}}_1^{L(j)} \tag{19}$$

In addition, Eq. (19) must be considered while expressing the time derivative of $\boldsymbol{u}_{A_1}^{L(j)}$ in $\mathbf{b}_{L(j)}$ using the assumed modes method. The time derivative of the elastic displacement at node A_1 has the form

$$\frac{\partial^{L(j)}}{\partial t}\left(\boldsymbol{u}_{A_1}^{L(j)}\right) = \dot{\xi}_1 \sum_{i=1}^{\mathrm{NM}_{L(j)}} \left[\phi_i'^{L(j)}\left(\boldsymbol{r}_{A_1}^{L(j)}\right)\eta_i^{L(j)}\right] \times \hat{\boldsymbol{n}}_1^{L(j)}$$

$$+ \sum_{i=1}^{\mathrm{NM}_{L(j)}} \phi_i^{L(j)}\left(\boldsymbol{r}_{A_1}^{L(j)}\right)\dot{\eta}_i^{L(j)} \tag{20}$$

The first term on the right side of Eq. (20) accounts for the translation of the contact point with respect to the body frame and the term under the summation yields the slopes due to elastic deflection. If a continuum representation of the mode shapes is available, computing the modal slopes is a straightforward task for any location on the flexible body. If the mode shape information is obtained from a finite element analysis, modal slopes at the nodes are already available, but interpolation functions must be used to obtain the modal displacements and slopes for locations that do not coincide with the nodes. The second term in Eq. (20) represents the elastic deformation rate in the absence of the rigid-body translational motion of A_1. Node A_2, however, does not undergo any rigid-body translation with respect to $\mathbf{b}_j$. Therefore,

$$\frac{\partial^j}{\partial t}\left(\boldsymbol{r}_{A_2}^j\right) = \mathbf{0} \tag{21}$$

$$\frac{\partial^j}{\partial t}\left[\boldsymbol{u}^j\left(\boldsymbol{r}_{A_2}^j, t\right)\right] = \sum_{i=1}^{\mathrm{NM}_j} \phi_i^j\left(\boldsymbol{r}_{A_2}^j\right)\dot{\eta}_i^j \tag{22}$$

Similar expressions can be written for the contact across the nodes B_1 and B_2, with B_1 and B_2 replacing A_1 and A_2 and ξ_2 replacing ξ_1.

In contrast to Eq. (19), the time derivative of $\boldsymbol{r}_{C_1}^{L(j)}$ in the local frame has the form

$$\frac{\partial^{L(j)}}{\partial t}\left(\boldsymbol{r}_{C_1}^{L(j)}\right) = \dot{\xi}_3 \hat{\boldsymbol{n}}_1^{L(j)} + \dot{\xi}_4 \hat{\boldsymbol{n}}_2^{L(j)} \tag{23}$$

where $\hat{\boldsymbol{n}}_2^{L(j)}$ is a unit vector orthogonal to $\hat{\boldsymbol{n}}_1^{L(j)}$ and is in the plane containing the parallel tracks in the undeformed configuration of body $L(j)$. The local derivative of the elastic deformation at node C_1 also has a different form:

$$\frac{\partial^{L(j)}}{\partial t}\left(\boldsymbol{u}_{C_1}^{L(j)}\right) = \dot{\xi}_3 \sum_{i=1}^{\mathrm{NM}_{L(j)}} \left[\phi_i'^{L(j)}\left(\boldsymbol{r}_{C_1}^{L(j)}\right)\eta_i^{L(j)}\right] \times \hat{\boldsymbol{n}}_1^{L(j)}$$

$$+ \dot{\xi}_4 \sum_{i=1}^{\mathrm{NM}_{L(j)}} \left[\phi_i'^{L(j)}\left(\boldsymbol{r}_{C_1}^{L(j)}\right)\eta_i^{L(j)}\right] \times \hat{\boldsymbol{n}}_2^{L(j)}$$

$$+ \sum_{i=1}^{\mathrm{NM}_{L(j)}} \phi_i^{L(j)}\left(\boldsymbol{r}_{C_1}^{L(j)}\right)\dot{\eta}_i^{L(j)} \tag{24}$$

Since C_2 is a node fixed on body j, the local time derivatives of the location of C_2 as well as the elastic deformation at that point will have forms similar to those in Eqs. (21) and (22). The constraint equations in Eqs. (18–24) and constraints similar to those in Eqs. (18–22) for the contact across the B_1 and B_2 nodes can then be scalarized and the constraint Jacobian matrix can be set up. If other constraints exist in the system, the nine scalar constraints from above yield only a part of the overall system Jacobian matrix. The velocity constraint equations can then be differentiated with respect to time to obtain the acceleration equations corresponding to these constraints. The system of equations presented in Sec. II must now be augmented with these constraints using Lagrange multipliers.

IV. Solution Method

Two choices exist for the solution of the constrained dynamic system. The first one is the elimination of $\dot{\xi}_1$, $\dot{\xi}_2$, $\dot{\xi}_3$, and $\dot{\xi}_4$ from the velocity constraint equations, so that only five constraints remain. Similarly, $\ddot{\xi}_1$, $\ddot{\xi}_2$, $\ddot{\xi}_3$, and $\ddot{\xi}_4$ can be eliminated from the acceleration constraint equations. This is straightforward, as will be shown in the next section using an example. The second approach, that of Hwang and Haug,[6] is to make ξ_1, ξ_2, ξ_3, and ξ_4 part of the generalized coordinates and consider the nine constraints directly. The first approach is preferred for implementing the present model into an existing multibody dynamics code. This is because the variables ξ_1, ξ_2, ξ_3, and ξ_4 are needed only for computing the elements of the constraint Jacobian matrix and do not affect the terms or the dimension of the unconstrained dynamics equations. These variables can be obtained by integrating the first-order differential equations for $\dot{\xi}_1$, $\dot{\xi}_2$, $\dot{\xi}_3$, and $\dot{\xi}_4$. The second approach, however, would require increasing the dimension of ν by 4 (or increasing the first-order equations by 8).

In both cases the incorporation of the constraints in a multibody program requires a systematic approach. These constraints can be combined with other constraints present in the system so that the constraint Jacobian matrix can be obtained for the whole system. Then, the dynamics equations with constraints can be written as

$$M(\nu)\dot{\nu} + G(\nu, \dot{\nu}) = F + J^T\lambda \tag{25}$$

where J is the constraint Jacobian matrix and λ represents a column matrix of Lagrange multipliers. A numerical algorithm such as a singular value decomposition[14] or a QR decomposition[15] is needed for solving the constraint equations. The reader is referred to Refs. 14 and 15 for details. The solution method then consists of solving the dynamics equations in Eq. (25) together with the constraints formed in Sec. III.

V. Illustrative Example

The three-dimensional motion of a system is simulated here to demonstrate the proposed approach. The problem is that of the translation of a three (noncollinear) legged rigid cart over a flexible plate. The cart is chosen to be rigid so that the salient features of the three-point contact model can be demonstrated. The cart (body j) and the plate [body $L(j)$] are the only bodies in the system [$j = 2$, $L(j) = 1$, and NB = 2]. Hinge 1 connects the plate to the ground whereas hinge 2 connects the plate and the cart. The plate has no rigid-body DOFs with respect to the inertial frame. Thus, $\mathrm{NT}_1 = \mathrm{NR}_1 = 0$. As discussed earlier, $\mathrm{NT}_2 = \mathrm{NR}_2 = 3$.

The plate is square with side $a = 25$ m and thickness $h = 0.01$ m, is made of aluminum (density $\mu = 2770$ kg/m^3, Young's modulus $E = 6.9 \times 10^{10}$ N/m^2, Poisson's ratio $\nu = 0.3$), and is simply supported on all of its edges. The cart has a mass of 100 kg and has the following principal inertias: $I_{xx} = I_{yy} = I_{zz} = 100$ kg $\cdot$ m^2. The cart mass center is the origin of $\mathbf{b}_2$, and the body frame axes are the principal inertia axes. The axes of the cart and plate reference frames are parallel in the absence of plate flexibility. Six DOFs are allowed across joint 2 connecting the cart and the plate. The coordinates of the contact points with respect to the cart reference frame are $A_2(-2\text{ m}, -2\text{ m}, -1\text{ m})$, $B_2(2\text{ m}, -2\text{ m}, -1\text{ m})$, and $C_2(0, 2\text{ m}, -1\text{ m})$.

The reference frame $\mathbf{b}_1$ for the plate is located as shown in Fig. 3, and the nominal translational motion of the cart is along the plate x axis ($\boldsymbol{n}_1^{L(j)} = \boldsymbol{b}_{11}$). Let the y and the z axes for the plate correspond to the $\hat{\boldsymbol{n}}_2^{L(j)} (= \boldsymbol{b}_{12})$ and the $\boldsymbol{b}_{13}$ axes, respectively. Then, the transverse deflection of the plate is along the z axis, such that $\boldsymbol{u}^1 = u(x, y, t)\boldsymbol{b}_{13}$. Using the assumed modes method and the simply supported mode shapes of a uniform square plate, the elastic displacement $u(x, y, t)$ can be expressed as

$$u(x, y, t) = \sum_{i=1}^{\infty}\sum_{k=1}^{\infty} \psi_{ik}(x, y)\gamma_{ik}(t) \tag{26}$$

where the mass-normalized mode shapes are given by[16]

$$\psi_{ik}(x, y) = \frac{2}{a\sqrt{\mu h}} \sin\left(\frac{i\pi x}{a}\right) \sin\left(\frac{k\pi y}{a}\right) \tag{27}$$

and γ_{ik} are their time-dependent amplitudes. The plate mode shapes are functions of both the spatial variables x and y. The plate modal equations are

$$\ddot{\gamma}_{ik} + \left[\left(\frac{\pi}{a}\right)^4 \frac{Eh^2}{12\mu(1-\nu^2)}(i^2 + k^2)^2\right]\gamma_{ik} = 0 \tag{28}$$

The double subscript on γ corresponds to the xy spatial dependency. These γ_{ik} can be related to the η as follows: $\eta_1 = \gamma_{11}$, $\eta_2 = \gamma_{21}$, $\eta_3 = \gamma_{12}$, $\eta_4 = \gamma_{22}$, etc. The expression inside the square brackets denotes the corresponding Ω^2 term, where Ω denotes the natural frequency.

The top view of the cart and the plate system at the simulation start is shown in Fig. 3. The p node is selected, on the plate, with the coordinates (8 m, 8 m, 0) in the body frame and the q node

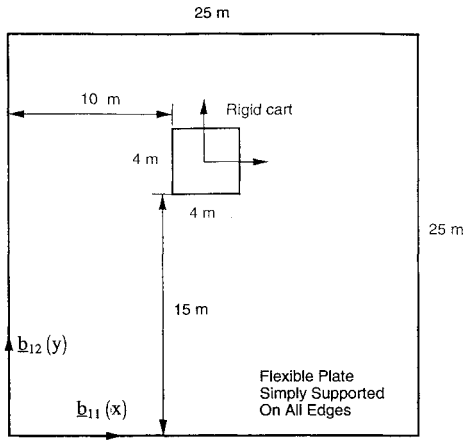

Fig. 3 Planar view of undeformed plate and cart system at simulation start.

coordinates in the cart reference frame are (−2 m, 0, 0). Thus, $(\boldsymbol{r}_q^j - \boldsymbol{r}_{A_2}^j) = \mathbf{b}_j^T[0\ 2\ 1]^T$.

Since hinge 1 does not permit any motion across it and all the six DOFs are available at hinge 2, let

$$y_i = y_i^{(2)}, \qquad \theta_i = \theta_i^{(2)} \qquad i = 1, 2, 3 \tag{29}$$

Also, let

$$\eta_i = \eta_i^{(1)}, \qquad i = 1, \ldots, \mathrm{NM}_1 \tag{30}$$

In addition, since the rotational motion of the cart is due only to the vibration of the flexible plate, we employ a small-angle assumption in computing the rotational transformation matrix between $\mathbf{b}_j$ and $\mathbf{b}_{L(j)}$. Let $\phi_{ip} = \phi_i(r_{px}, r_{py})$, where $[r_{px}\ r_{py}\ 0]^T = \mathbf{b}_{L(j)} \cdot \boldsymbol{r}_p$. For a system with the parameters given in this section, neglecting higher order terms, the scalar velocity constraints for the contact across the node pair A_1 and A_2 are given by

$$\dot{\xi}_1 = (1 - y_3)\sum_{i=1}^{\mathrm{NM}_1} \frac{\partial\phi_{ip}}{\partial x}\dot{\eta}_i - 2\frac{\partial u_p}{\partial x}\dot{\theta}_1 - \dot{\theta}_2 + 2\dot{\theta}_3 + \dot{y}_1 + \frac{\partial u_p}{\partial y}\dot{y}_3 \tag{31}$$

$$0 = (1 - y_3)\sum_{i=1}^{\mathrm{NM}_1} \frac{\partial\phi_{ip}}{\partial y}\dot{\eta}_i + \left(1 + 2\frac{\partial u_p}{\partial y}\right)\dot{\theta}_1 + \dot{y}_2 - \frac{\partial u_p}{\partial x}\dot{y}_3 \tag{32}$$

$$\frac{\partial u_{A_2}}{\partial x}\dot{\xi}_1 = \sum_{i=1}^{\mathrm{NM}_1}\left[(y_2 - 2)\frac{\partial\phi_{ip}}{\partial y} + y_1\frac{\partial\phi_{ip}}{\partial x}\right]\dot{\eta}_i + \left(\frac{\partial u_p}{\partial y} - 2\right)\dot{\theta}_1 + \frac{\partial u_p}{\partial x}(\dot{\theta}_2 - 2\dot{\theta}_3) - \frac{\partial u_p}{\partial y}\dot{y}_1 + \frac{\partial u_p}{\partial x}\dot{y}_2 + \dot{y}_3 \tag{33}$$

where the notation

$$\frac{\partial u_p}{\partial x} = \sum_{i=1}^{\mathrm{NM}_1}\frac{\partial\phi_{ip}}{\partial x}\eta_i, \qquad \frac{\partial u_p}{\partial y} = \sum_{i=1}^{\mathrm{NM}_1}\frac{\partial\phi_{ip}}{\partial y}\eta_i \tag{34}$$

has been employed for brevity. Elimination of $\dot{\xi}_1$ using Eq. (31) is straightforward. If the travel direction is not along one of the body frame axes, the equation for $\dot{\xi}_1$ can be obtained by dot multiplying Eq. (18) with $\hat{\boldsymbol{n}}_1^{L(j)}$. Similar expressions can be written for the contact across the B and C node pairs and $\dot{\xi}_2$, $\dot{\xi}_3$, and $\dot{\xi}_4$ can similarly be eliminated. We observe from Eq. (31) that $\dot{\xi}_1$ is not the only variable that can be selected for elimination. However, this choice is preferred based on the discussion in Sec. IV.

The initial values for the system variables are computed corresponding to $\eta_1 = -20\sqrt{\text{kg}}\cdot\text{m}$ and $A_1(10\text{ m}, 15\text{ m}, 0)$. The system response to these initial conditions is shown in Figs. 4a–4d: Fig. 4a shows the location of the cart mass center with respect to the origin

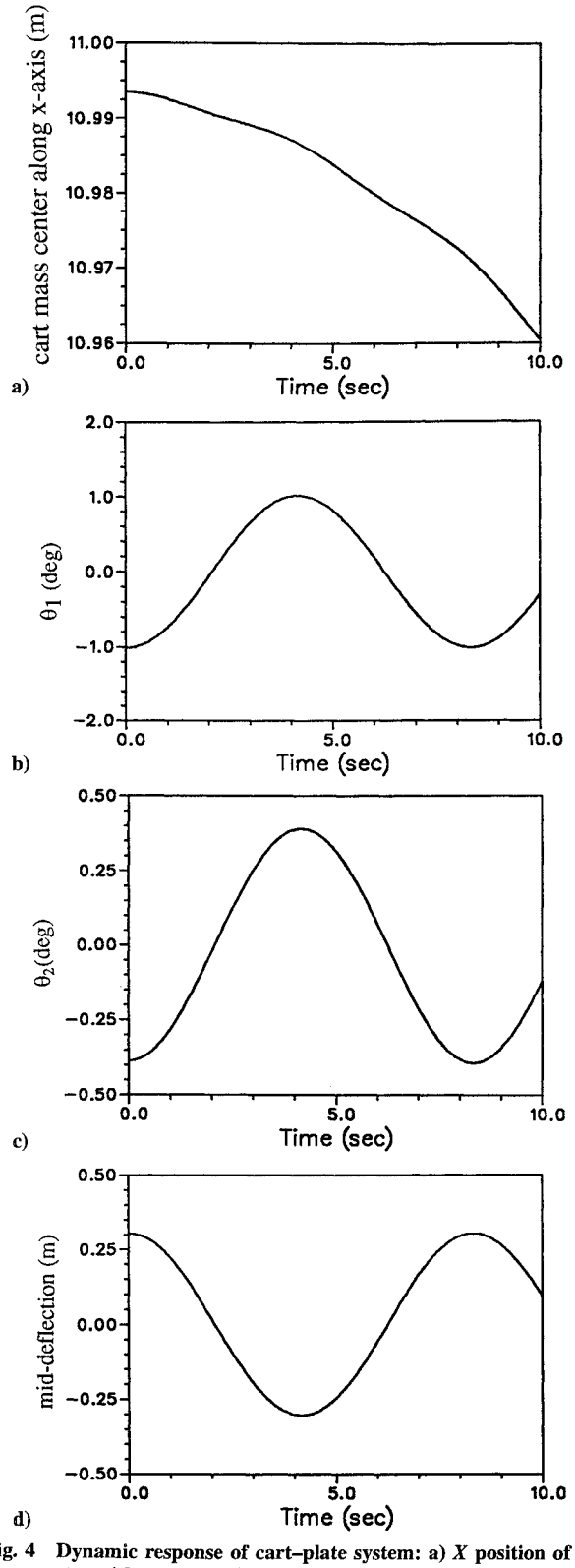

Fig. 4 Dynamic response of cart–plate system: a) X position of cart mass center with respect to inertial frame; b) cart roll, rotation about plate X axis; c) cart pitch, rotation about plate Y axis; and d) plate midpoint deflection.

of the plate reference frame (also the inertial frame here) along the plate x axis; Figs. 4b and 4c show the 1–2 angles corresponding to a 1–2–3 Euler sequence between the cart and the inertial frame (for the small rotations considered here, these correspond to the roll and pitch motions of the cart with respect to the inertial frame); Fig. 4d shows the deflection of the midpoint on the plate. Although the first four modes of the plate were used in the simulation, it is clear that the interaction between modes is not significant and only the first mode dominates.

The responses shown in Figs. 4a–4d conform to expectations. The combination of the initial location of the cart (the top view is shown in Fig. 3), the fact that the first mode of vibration is like a bubble stretched over the square plate, and the initial positive y deflection result in an initial negative roll and pitch for the cart. This is apparent in Figs. 4b and 4c. This is also the reason for the downhill motion of the cart shown in Fig. 4a. As the plate starts vibrating, the roll and pitch motions oscillate about their equilibrium values. With the exception of the translation of the cart, all the motions are harmonic. The translational motion of the cart is not harmonic because there is no restraint in that direction.

The simulation of constrained dynamic systems often requires the use of a constraint violation stabilization scheme (Yoon et al.[17]). This is especially important in the context of the present model because of the use of constraints. The numerical example presented by Yoon et al.[17] is that of a point mass rotating in a unit circle. The example considered here is much more complex. Energy conservation was violated soon after simulation start for the cart–plate system. A combination of geometric constraint control and energy constraint control, recommended by Yoon et al.,[17] was then implemented, with reasonable success. The success appeared to depend on system properties such as the cart mass and inertia, plate stiffness, etc.

VI. Implementation in Multibody Dynamics Codes

The recursive kinematics and dynamics formulations presented in Sec. II are the same as those presented in Ref. 4 and implemented in TREETOPS[4] and GRASP.[18] Both these software codes currently do not model constraints of the form presented in Sec. III. Inclusion of these constraints in the above codes will enable the modeling of open- and closed-loop dynamic systems with single-point-contact as well as multi-point-contact joints. The changes needed are essentially in the formulation of constraints. A module can be created for implementing the constraints presented here. The variables $\dot{\xi}_1$, $\dot{\xi}_2$, $\dot{\xi}_3$, and $\dot{\xi}_4$ and their time derivatives can be eliminated inside this module. However, as mentioned in Sec. IV, first-order equations for $\dot{\xi}_1$, $\dot{\xi}_2$, $\dot{\xi}_3$, and $\dot{\xi}_4$ must now be appended to the system dynamic equations.

It is assumed that the component modal analysis for each elastic body is performed prior to using this model, as is the custom with the multibody dynamics codes TREETOPS,[4] DISCOS,[5] and GRASP.[18] When the component modes are obtained from a finite element analysis, the mode shape data for body $L(j)$ must be available for all the nodes across which possible body j motion occurs, so that the terms on the right side of Eq. (20) can be obtained by interpolation, which must be performed inside the multibody code.

An extension to the model is allowing more than one relative DOF between the bodies. The cart in our example can be made to have up to three DOFs with respect to the plate—two translations and one rotation—by relaxing the assumption on the translational direction. This can be achieved by introducing two variables each to describe the x–y coordinates for the contact across A_1 and A_2 and B_1 and B_2. Recall that two coordinates were already introduced for the contact across C_1 and C_2. The number of new configuration variables describing the contact will now be six. Once again, these variables are not independent of the generalized coordinates presented in Sec. II and can be eliminated using six of the nine scalar constraints. The remaining three constraints when solved together with the six DOFs across the body pair will yield the desired three relative DOFs between the cart and the plate.

VII. Application

The current designs for the construction of the International Space Station Alpha (ISSA) call for an on-orbit incremental buildup. The use of a Shuttle Remote Manipulator System (SRMS), a Mobile Transporter (MT), and a Space Station Remote Manipulator System (SSRMS) are planned for the on-orbit ISSA assembly. The MT is slated for use during the buildup as well as after the completion of the assembly of the ISSA. The MT, shown in Fig. 5 (Ref. 19), has two roller suspension units (RSUs) and a linear drive unit (LDU) that are fixed to the MT structure and traverses the space station along a pair of parallel rails that are fixed on the ISSA. The RSUs are spring loaded so that contact is maintained between the wheels and the rails

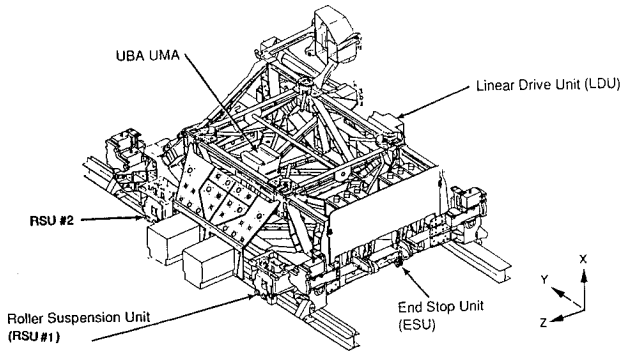

Fig. 5 Mobile transporter.

at all times. The ISSA and the links of the robot arm's SRMS and SSRMS are flexible enough that rigid-body models do not suffice.

The dynamic interactions of the flexible MT–ISSA system cannot be modeled using the multibody dynamics tools that are currently available.[9,12] It is now possible to simulate the MT–ISSA dynamics using the approach presented here by modeling the contact between each set of RSUs (or LDU) and the ISSA as a single point contact. A controller has already been designed for the translational motion control of the MT. An analysis of the MT controller at the system level can now be made possible by incorporating the present model into the existing multibody dynamics codes.

VIII. Conclusion

A method is presented here for modeling the translational motion between two flexible bodies with three points of contact. The method consists of first allowing all the six degrees of freedom between the bodies and then imposing the constraints that account for moving contact points. The body flexibility is assumed to be small and it is represented using a set of assumed modes. Modal data from finite element analyses can be used. To the best of the author's knowledge, this is the first time a three-point (noncollinear) contact between two adjacent flexible bodies possessing a nonprescribed translational degree of freedom has been modeled. Simulation results presented for the case of a three-legged rigid body traveling on a flexible plate demonstrate the interaction dynamics of the combined system. This system is used as an example to provide insight into the nature of the problem.

The model development is presented in a multibody format so that this model can be incorporated, as an extension, into existing multi-flexible-body dynamics codes. The steps needed for implementation are outlined. The Mobile Transporter–Space Station system is a direct application for the present model. Extension to the case of three relative degrees of freedom between two flexible bodies, also with a three-point contact, is discussed.

Acknowledgments

This paper is based on work performed for the NASA Space Station Freedom Program Office under Contract NASW-4300. The author gratefully acknowledges the support of Jalal Mapar, Manager, Integrated Performance Analysis. The author also thanks the anonymous reviewers for their valuable comments.

References

[1]Banerjee, A. K., "Block-Diagonal Equations for Multibody Elastodynamics with Geometric Stiffness and Constraints," *Journal of Guidance, Control, and Dynamics*, Vol. 16, No. 6, 1993, pp. 1092–1100.

[2]Kim, S.-S., and Haug, E. J., "A Recursive Formulation for Flexible Multibody Dynamics, Part I: Open-Loop Systems," *Computer Methods in Applied Mechanics and Engineering*, Vol. 71, 1988, pp. 293–314.

[3]Shabana, A. A., "Constrained Motion of Deformable Bodies," *International Journal for Numerical Methods in Engineering*, Vol. 32, 1991, pp. 1813–1831.

[4]Singh, R. P., VanderVoort, R. J., and Likins, P. W., "Dynamics of Flexible Bodies in a Tree Topology—A Computer-Oriented Approach," *Journal of Guidance, Control, and Dynamics*, Vol. 8, No. 5, 1985, pp. 584–590.

[5]Bodley, C. S., Devers, A. D., Park, A. C., and Frisch, H. P., "A Digital Computer Program for the Dynamic Interaction Simulation of Controls and Structures (DISCOS)," Vols. 1 and 2, NASA TP-1219, 1978.

[6]Buffinton, K. W., and Kane, T. R., "Dynamics of a Beam Moving Over Supports," *International Journal of Solids and Structures*, Vol. 21, No. 7, 1985, pp. 617–643.

[7]Li, D., and Likins, P. W., "Dynamics of a Multibody System with Relative Translation on Curved, Flexible Tracks," *Journal of Guidance, Control, and Dynamics*, Vol. 10, No. 3, 1987, pp. 299–306.

[8]Hwang, R.-S., and Haug, E. J., "Translational Joints in Flexible Multibody Dynamics," TR-R-6, Univ. of Iowa, Iowa City, IA, 1989.

[9]Messac, A., and Herman, D., "Dynamics of Multibody Flexible Systems with Multi-Point Joints," 42nd Congress of the International Astronautical Federation, Paper IAF-91-292, Montreal, Canada, Oct. 1991.

[10]Fryba, L., *Vibrations of Solids and Structures under Moving Loads*, Noordhoff, Groningen, The Netherlands, 1972.

[11]Olsson, M., "Finite Element Modal Co-ordinate Analysis of Structures Subjected to Moving Loads," *Journal of Sound and Vibration*, Vol. 99, No. 1, 1985, pp. 1–12.

[12]Messac, A., Herman, D., and Malchow, H., "A Space Station Freedom Mobile Transporter Simulation," The Charles Stark Draper Lab., Rept. SS-92-05, Cambridge, MA, 1992.

[13]Meirovitch, L., *Computational Methods in Structural Dynamics*, Sijthoff and Noordhoff, Alphan aan den Rijn, The Netherlands, 1980.

[14]Singh, R. P., and Likins, P. W., "Singular Value Decomposition for Constrained Multibody Systems," *Journal of Applied Mechanics*, Vol. 52, No. 4, 1985, pp. 943–948.

[15]Kim, S. S., and Vanderploeg, M. J., "QR Decomposition for the State Space Representation of Constrained Mechanical Dynamic Systems," *Journal of Mechanisms, Transmissions and Automation in Design*, Vol. 108, June 1986, pp. 183–188.

[16]Timoshenko, S., Young, D. H., and Weaver, W., Jr., *Vibration Problems in Engineering*, Wiley, New York, 1974.

[17]Yoon, S., Howe, R. M., and Greenwood, D. T., "Constraint Violation Stabilization Using Gradient Feedback in Constrained Dynamics Simulation," *Journal of Guidance, Control, and Dynamics*, Vol. 15, No. 6, 1992, pp. 1467–1474.

[18]*GRASP Theory Manual*, Grumman Space Station Integration Div., Reston, VA, 1991.

[19]Anon., "Dynamic Analysis and Control Design for the Space Station Mobile Transporter," Astro Aerospace Corp., Doc. AD-6069-105, Carpentaria, CA, Oct. 1992.